China Ocean Eng., Vol. 30, No. 2, pp. 177 – 192

DOI 10.1007/s13344-016-0010-1, ISSN 0890-5487

An Irregular Wave Generating Approach Based on naoe-FOAM-SJTU Solver*

SHEN Zhi-rong (沈志荣) and WAN De-cheng (万德成)[1]

State Key Laboratory of Ocean Engineering, School of Naval Architecture, Ocean and Civil Engineering, Shanghai Jiao Tong University, Collaborative Innovation Center of Advanced Ship and Deep-Sea Exploration, Shanghai 200240, China

(Received 28 November 2013; received revised form 13 January 2015; accepted 20 March 2015)

ABSTRACT

In this paper, a wave generating approach for long-crest irregular waves in a numerical tank by our in-house solver naoe-FOAM-SJTU is presented. The naoe-FOAM-SJTU solver is developed using an open source tool kit, OpenFOAM. Reynolds-averaged Navier–Stokes (RANS) equations are chosen as governing equations and the volume of fluid (VOF) is employed to capture the two phases interface. Incoming wave group is generated by imposing the boundary conditions of the tank inlet. A spectrum based correction procedure is developed to make the measured spectrum approaching to the target spectrum. This procedure can automatically adjust the wave generation signal based on the measured wave elevation by wave height probe in numerical wave tank. After 3 to 4 iterations, the measured spectrum agrees well with the target one. In order to validate this method, several wave spectra are chosen and validated in the numerical wave tank, with comparison between the final measured and target spectra. In order to investigate a practical situation, a modified Wigley hull is placed in the wave tank with incoming irregular waves. The wave-induced heave and pitch motions are treated by Fourier analysis to obtain motion responses, showing good agreements with the measurements.

Key words: *irregular wave*; *wave spectrum*; *RANS*; *VOF*; *OpenFOAM*; *naoe-FOAM-SJTU solver*

1. Introduction

As a research tool, Computational Fluid Dynamics (CFD) has been widely used in the field of marine and offshore engineering during the past decade. Many researchers have been focusing on CFD computations of the seakeeping in the regular wave and validation with experiments. Sato *et al.*(1999) predicted heave and pitch motions of Wigley hull and Series 60 in regular waves, treating the motions of ship as body force in N-S equations. Orihara and Miyata (2003) studied a container ship in head waves based on an overlapping grid system. The emphasis was placed on the added resistance and motion responses. Yang *et al.* (2006) simulated both internal sloshing liquid of an LNG carrier and outer sea waves around the ship by VOF method simultaneously. An incompressible Euler/Navier Stokes

* This work was financially supported by National Natural Science Foundation of China (Grant Nos. 51379125, 51411130131, 11432009, and 51490675), the Chang Jiang Scholars Program (Grant No. T2014099), the Innovative Special Project of Numerical Tank of Ministry of Industry and Information Technology of China (Grant No. 2016-23), the Foundation of State key Laboratory of Ocean Engineering (Grant No. GKZD010065), and the Program for Professor of Special Appointment (Eastern Scholar) at Shanghai Institutions of Higher Learning (Grant No. 2013022), center for HPC at Shanghai Jiao Tong University, and Lloyd's Register Foundation (LRF).

1 Corresponding author. E-mail: dcwan@sjtu.edu.cn

discretized by finite element method was solved for both internal and outside regions and an arbitrary Lagrangian-Eulerian (ALE) was used to treat the motions of ship. Carrica *et al.* (2007) generated regular head waves by a single-phase level-set method and simulated large-amplitude motions of DTMB model 5512 based on overset grid technique. Although most of the CFD researches focus on the conditions in regular waves, they have limitations on the simulations of real sea environment. Real sea environment contains various wave frequencies while regular wave has only one. For the regular wave based method, each wave frequency requires one run and a complete curve of motion response requires at least a decade of computations or tests. In recent years, more emphases have been placed on the CFD computations of irregular waves and fluid-structure interaction. Carrica *et al.* (2008) simulated irregular quartering waves to study broaching event by overset technique and finite-difference method. Mousaviraad *et al.* (2010) developed transient and harmonic wave group procedures to predict RAO by a single-run.

However, compared with the conventional potential methods, CFD methods suffer from severe numerical dissipation. For instant, the amplitude of incident wave is decreasing along the direction of propagation if the mesh density is not sufficiently enough. The resulting amplitude is far away from the target value when a wave crest reaches the object. One solution is to increase the mesh density near the surface along the wave propagation direction. However, the disadvantage of this solution is the accompanying smaller time step and increasing computational time. The problem is much more severe for irregular wave because it contains a wide range of wave frequencies. It is difficult to maintain the amplitudes of all wave components.

In this paper, we develop a wave spectrum based correction approach for irregular wave generation. The method can maintain the wave amplitudes to the target values when the waves approach to the floating object. This approach is first used in the physical wave tank. It is a procedure of iteration. It automatically adjusts the input wave spectrum according to the measured wave elevation in numerical tank. The iteration is converged after 3 to 4 iterations and the measured spectrum can closely agree with the target. Test cases with several wave spectra are included to validate this method. At last, a modified Wigley hull is placed in the wave tank with incoming irregular waves. Motion responses are investigated and compared with existing measurements.

The open source toolbox, OpenFOAM, is utilized as a simulation platform to carry out the study. Since OpenFOAM is free and the source code is open to everyone, it has been widely used in the field of ship and ocean engineering. Jacobsen *et al.* (2012) developed a wave generation toolbox in OpenFOAM to generate a variety of wave types by relaxation approach. Chen *et al.* (2014) applied OpenFOAM to investigate wave-structure interaction of a vertical surface piercing cylinder. Emphasis was placed on the wave loads on the cylinder and comparison with the experiments. The comparison showed good agreements. Higuera *et al.* (2013) developed a wave generation and active wave absorption boundary conditions in OpenFOAM. The active absorption boundary did not increase the computational domain. It was proved more effective than sponge layer method. The method was able to maintain the water level on long simulations.

The computations in this work are carried out by a two-phase incompressible Reynolds-Average Navier–Stokes (RANS) solver, naoe-FOAM-SJTU (Shen and Wan, 2013). This solver was developed based on OpenFOAM. The structure of the solver is shown in Fig. 1. In addition to the native

OpenFOAM libraries such as finite volume method, volume of fluid method, deforming mesh, we developed a wave generation and damping module and a 6-degree-of-freedom (6DoF) module. After the two modules are combined with the native OpenFOAM libraries, this solver can be applied not only to the simulations of wave-structure interaction but also to the predictions of motion responses. In the previous work, this solver has been validated for a range of ship and offshore hydrodynamic problems (Cao and Wan, 2015; Shen and Wan, 2013; Shen *et al.*, 2014). In this work, the wave generation module is extended for a wave spectrum based correction approach. The details can be found in the following section.

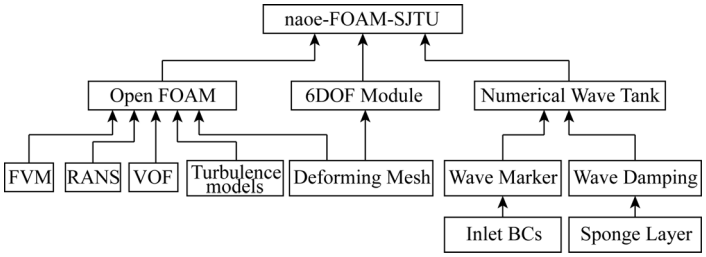

Fig. 1. Structure of naoe-FOAM-SJTU solver.

2. Numerical Methods

2.1 Governing Equations

The incompressible Reynolds-Averaged Navier–Stokes equations are the governing equations, written as:

$$\nabla\cdot\boldsymbol{U}=0\,; \tag{1}$$

$$\frac{\partial\rho\boldsymbol{U}}{\partial t}+\nabla\cdot\left[\rho\left(\boldsymbol{U}-\boldsymbol{U}_{\mathrm{g}}\right)\boldsymbol{U}\right]=-\nabla p_{\mathrm{d}}-\boldsymbol{g}\cdot\boldsymbol{x}\nabla\rho+\nabla\cdot\left(\mu_{\mathrm{eff}}\nabla\boldsymbol{U}\right)+\left(\nabla\boldsymbol{U}\right)\cdot\nabla\mu_{\mathrm{eff}}+f_{\mathrm{s}}+f_{\sigma}\,, \tag{2}$$

where, $\boldsymbol{U}$ is the velocity field; $\boldsymbol{U}_{\mathrm{g}}$ is the velocity of grid nodes; $p_{\mathrm{d}}=p-\rho\boldsymbol{g}\cdot\boldsymbol{x}$ is the dynamic pressure, subtracting hydrostatic component $\rho\boldsymbol{g}\cdot\boldsymbol{x}$ from total pressure p; ρ is the mixture density with two phases; $\boldsymbol{g}$ is the gravitational acceleration vector; $\mu_{\mathrm{eff}}=\rho(\nu+\nu_{\mathrm{t}})$ is the effective dynamic viscosity, in which ν and ν_{t} are the kinematic viscosity and the eddy viscosity respectively; ν_{t} is obtained by $k-\omega$ SST turbulence model (Menter *et al.*, 2003). f_{s} is the source term of sponge layer to damping wave reflections. f_{σ} is the source term of the surface tension. Both of the two source terms will be discussed in the following sections. The momentum and continuity equations are solved by the pressure-implicit split-operator (PISO) algorithm (Issa, 1986), utilizing collocated grid introduced by Rhie and Chow (1983) to remove pressure oscillations.

A VOF method with artificial compression techniques is applied to capture free surface interface. Only a brief introduction of this method is presented here and the details can be referred to Rusche (2002) and Berberović *et al*. (2009). The VOF transport equation is expressed as:

$$\frac{\partial\alpha}{\partial t}+\nabla\cdot\left[\left(\boldsymbol{U}-\boldsymbol{U}_{\mathrm{g}}\right)\alpha\right]+\nabla\cdot\left[\boldsymbol{U}_{\mathrm{r}}\left(1-\alpha\right)\alpha\right]=0\,, \tag{3}$$

where α is the volume of fraction, indicating the relative proportion of fluid volume in each cell and its value is bounded between zero and one. The definition of α is listed in Eq. (4). The term $\boldsymbol{U}_{\mathrm{r}}$ in Eq. (3) is the velocity field used to compress the interface. Because of the term $(1-\alpha)\alpha$, $\boldsymbol{U}_{\mathrm{r}}$ takes effect only on the surface interface. The detailed expression of $\boldsymbol{U}_{\mathrm{r}}$ can be found at Berberović *et al.* (2009). Besides, the surface tension term in Eq. (2) is defined as $f_{\sigma}=\sigma\kappa\nabla\alpha$, where σ is the surface tension coefficient, being 0.07 kg/s^2 in present work. κ is the curvature of surface interface, determined by the volume of fraction α, as shown in Eq. (5).

$$\begin{cases}\alpha=0 & \text{air}\\ \alpha=1 & \text{water}\\ 0<\alpha<1 & \text{interface}\end{cases} \tag{4}$$

$$\kappa=-\nabla\cdot\left(\nabla\alpha/\left|\nabla\alpha\right|\right) \tag{5}$$

2.2 Wave Generation Module

The wave generation method is applied by imposing the boundary conditions of α in VOF Eq. (3) and $\boldsymbol{U}(u,v,w)$ in RANS Eq. (2). The irregular waves are assumed as a superposition of a series of linear airy waves.

$$\begin{cases}\zeta(x,t)=\sum_{i=1}^{\infty}a_i\cos(k_i x-\omega_{\mathrm{e}}t+\varphi_i)\\ u(x,z,t)=U_0+\sum_{i=1}^{\infty}a_i\omega_i\mathrm{e}^{k_i z}\cos\left(k_i x-\omega_{ei}t+\varphi_i\right)\\ w(x,z,t)=\sum_{i=1}^{\infty}a_i\omega_i\mathrm{e}^{k_i z}\sin\left(k_i x-\omega_{ei}t+\varphi_i\right)\end{cases} \tag{6}$$

where, $\zeta(x,t)$ is transient wave elevation; $u(x, z, t)$ and $w(x, z, t)$ are the velocity components in the x and z directions, respectively; the subscript i is the index of each wave components; a_i is the wave amplitude; k_i is the wave number; ω_i is the natural frequency of wave and ω_{ei} the called encounter frequency, given by

$$\omega_{ei}=\omega_i+k_i U_0\cos\beta, \tag{7}$$

where, β is the wave direction, which is zero in this paper, representing head wave; U_0 is the forward speed of a ship. Eq. (7) can be rewritten as:

$$f_{ei}=f_i+2\pi f_i^2 U_0\cos\beta/g, \tag{8}$$

where $f_{ei}=\omega_{ei}/(2\pi)$ and $f_i=\omega_i/(2\pi)$.

The wave generation method imposes the boundary conditions of the velocity $\boldsymbol{U}$ and α at the inlet. As for the velocity boundary condition, the expressions of u, w in Eq. (6) can be directly adopted as a Dirichlet boundary condition. The boundary condition of α is more complicated than those of u and w. In the cell faces of the boundary located below the interface of $\zeta(x,t)$, $\alpha=0$, otherwise, $\alpha=1$.

In the cell faces which are crossing the interface of $\zeta(x,t)$, each face is divided into two parts: one above $\zeta(x,t)$ and the other below it. Since α is the volume ratio of each cell, it can be simplified as:

$$\alpha = \frac{S_{\mathrm{b}}}{S_0}, \tag{9}$$

where, S_0 is the total area of the cell face and S_{b} is the area of the part below $\zeta(x,t)$.

In the computation of ocean structures that have forward speed, the reference frame of the numerical of tank keeps moving with the objects. Hence the wave spectrum $S(\omega)$ is required to transform from the natural frequency ω to the encounter frequency ω_{e}:

$$S(\omega_{\mathrm{e}}) = \frac{S(\omega)}{1+\frac{2\omega}{g}U_0\cos\beta}, \tag{10}$$

where, $S(\omega_{\mathrm{e}})$ is the spectral density function based on the encounter frequency ω_{e}; U_0 is the forward speed of the moving object; β is the wave direction and g is the gravitational acceleration.

The wave amplitude a_i of each component is calculated by spectral density function $S(\omega_{\mathrm{e}})$:

$$a_i = \sqrt{2S(\omega_{\mathrm{e}i})\mathrm{d}\omega_{\mathrm{e}i}}, \tag{11}$$

The phase of each component can be chosen randomly. In this work, it is calculated by:

$$\varphi_i = k_i\sum_{l=1}^{i}\lambda_1, \tag{12}$$

where, φ_i is the phase used by Eq. (6); λ_1 is the wave length and k_i is the wave number.

The results of wave elevation and motion are processed through Fourier analysis. The frequency of each wave component can be given by,

$$f_i = n_i f_{\mathrm{f}}, \tag{13}$$

where f_{f} is called fundamental frequency and n_i is a positive integer. f_i can be natural wave frequency, and the angular frequency is $\omega_i = 2\pi f_i$. The sampling period T_{s} is defined by:

$$T_{\mathrm{s}} = \frac{1}{f_{\mathrm{f}}}. \tag{14}$$

The wave period of each component wave is defined as:

$$T_i = \frac{1}{f_i} = \frac{1}{n_i f_{\mathrm{f}}} \tag{15}$$

Combine Eqs. (14) and (15), we can have

$$\frac{T_{\mathrm{s}}}{T_i} = \frac{1/f_{\mathrm{f}}}{1/(n_i f_{\mathrm{f}})} = n_i. \tag{16}$$

Hence T_{s} covers integral multiple of T_i. The spectral leakage is ideally zero if window functions are simply used over one T_{s}.

The measured wave amplitude and spectrum of each component over one T_{s} can be obtained by:

$$a(\omega_i)=\frac{2}{T_s}\sqrt{C^2(\omega_i)+Q^2(\omega_i)}\,; \tag{17}$$

$$S(\omega_i)=\frac{C^2(\omega_i)+Q^2(\omega_i)}{\pi T_s}, \tag{18}$$

where $C(\omega_i)$ and $Q(\omega_i)$ are defined as:

$$\begin{cases} C(\omega_i)=\int_0^{T_s}\zeta_z(t)\cos(\omega_i t)\mathrm{d}t \\ Q(\omega_i)=-\int_0^{T_s}\zeta_z(t)\sin(\omega_i t)\mathrm{d}t \end{cases} \tag{19}$$

where $\zeta_z(t)$ is the measured wave evaluation at a specified location; T_s is the sampling period; ω_i is the wave frequency of each component.

2.3 Spectrum Correction

A wave spectrum based correction procedure is introduced to correct the wave generation signal during the computation. This method makes the measured spectrum match the target at the location of wave probe. This procedure can be expressed as:

$$S_{I2}(\omega_i)=\frac{S_{I1}(\omega_i)\cdot S_T(\omega_i)}{S_M(\omega_i)}, \tag{20}$$

where $S_{I1}(\omega_i)$ is the input spectrum; $S_{I2}(\omega_i)$ is the corrected spectrum, used to generate irregular waves for the next sampling period; $S_T(\omega_i)$ is the target spectrum and $S_M(\omega_i)$ is the measured spectrum in wave tank.

A wave height probe is set up at the numerical wave tank. During the computation, the probe records the transient wave elevation and computes the spectrum $S_M(\omega_i)$ by Eq. (18), which is returned to the wave maker after correction. The wave maker is controlling all wave generation parameters and correcting the input spectrum based on Eq. (20). In addition, a relaxation factor is introduced in this process in order to improve the stability and convergence of this algorithm:

$$S'_{I2}(\omega_i)=\lambda S_{I2}(\omega_i)+(1-\lambda)S_{I1}(\omega_i), \tag{21}$$

where $\lambda=0.5$ in this work. The wave maker replaces the old spectrum $S_{I1}(\omega_i)$ with the corrected $S'_{I2}(\omega_i)$. After 3 to 4 iterations, the measured spectrum $S_M(\omega_i)$ is approaching to target $S_T(\omega_i)$. Finally, we can use the corrected input spectrum $S'_{I2}(\omega_i)$ to generate irregular waves and achieve $S_T(\omega_i)$ at the location of wave height probe. The flow chart of this procedure is shown in Fig. 2.

Fig. 3 illustrates the code structure of the wave generation module. The module is developed based on OpenFOAM, written by the orient-object programming (OPP) language, C++. All the nodes demonstrated in this figure are encapsulated as classes. There are two nodes, *wave probe* and *wave maker*, directly called by the main function of the CFD solver. The *wave probe* can measure the wave elevation and computes the measured spectrum. The *wave maker* is the controller of the wave maker module. It declares an abstract base class named *wave theory*, which derives three wave generation

methods, *regular*, *solitary* and *irregular waves*. The first two will not be discussed in this paper since they are not applied in this work. Instead, we pay attention to the *irregular wave*. In this class, it declares an abstract base class named *wave spectrum*, which derives several commonly used spectra, such as JONSWAP, ISSC, and other Pierson–Moskowitz (P-M) based spectra. The *wave spectrum* calculates spectral density functions, wave amplitudes and phases and returns them to *irregular wave* class. In addition, *irregular wave* also declares a class to correct spectrum, which receives target spectrum from *irregular wave* and measured spectrum from *wave probe,* and then returns the corrected spectrum back to the controller, *wave maker*.

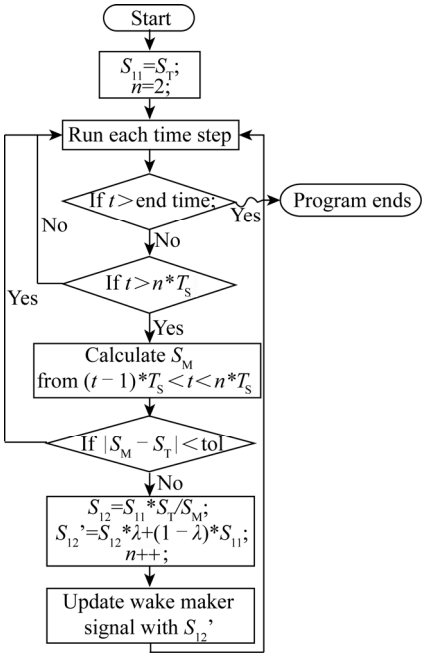

Fig. 2. Flow chart of corrector algorithm.

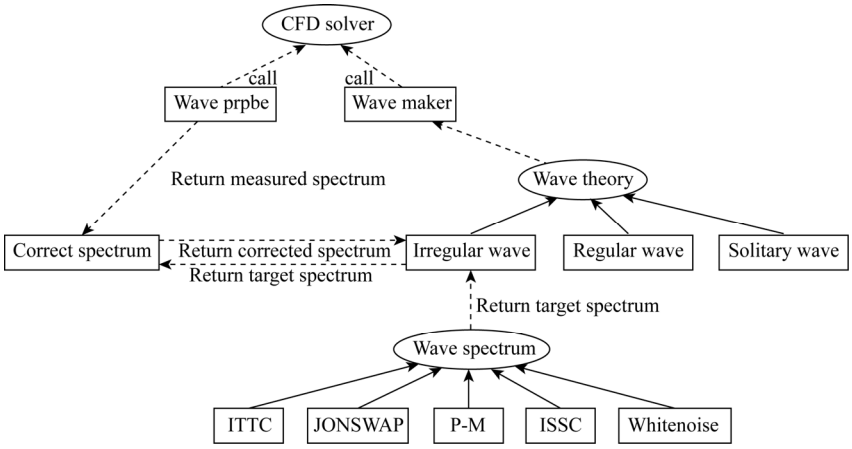

Fig. 3. Code structure of wave generation module.

2.4 Wave Damping

In order to absorb the wave reflection from outlet, a damping zone, also called sponge layer (Larsen and Dancy, 1983), is setup at the end of the tank to avoid the wave reflection. The sponge layer method was used in previous work (Cao *et al.*, 2011) and worked effectively. The source term f_s is added in Eq. (2) to absorb wave at the exit of wave tank. The term is denoted as:

$$f_s(x)=\begin{cases}-\rho\alpha_s\left(\dfrac{x-x_s}{L_s}\right)^2(\boldsymbol{U}-\boldsymbol{U}_{\text{ref}}) & \text{inside sponge layer}\\ 0 & \text{outside sponge layer}\end{cases} \tag{22}$$

where x_s is the start position of sponge layer; x is the position of mesh cells located in sponge layer. L_s is the length of layer; α_s is a dimensionless artificial viscosity parameter to control wave damping effect. α_s is 20 in current study. A reference velocity is $\boldsymbol{U}_{\text{ref}}$ included in the expression of sponge layer to dampen the velocity we specify the velocity at the exit and keep mass conversation of the computational domain.

3. Test Conditions

3.1 JONSWAP and ISSC Spectra

In this section, ISSC and JONSWAP spectra (Faltinsen, 1993) are chosen to generate the irregular waves.

ISSC (International Ship and Offshore Structures Congress) spectrum is recommended by the 15th ITTC (International Towing Tank Conference) for fully developed open sea condition:

$$S(\omega)=0.1107H_s^2\frac{\bar{\omega}^4}{\omega^5}\exp\left[-0.4427\left(\bar{\omega}/\omega\right)^4\right] \tag{23}$$

where $\bar{\omega}=2\pi/T_1$, T_1 is the mean wave period. $\bar{\omega}=1.296\omega_p$, $\omega_p=2\pi/T_p$ and T_p is the wave peak period. H_s is the significant wave height defined as the mean of the one third highest waves.

JONSWAP (Joint North Sea Wave Project) is one of the most frequently used spectra. The 17th ITTC recommended the JONSWAP spectrum for a limited fetch:

$$S(\omega)=319.34\frac{H_s^2}{T_p^4\omega^5}\exp\left[-\frac{1948}{\left(T_p\omega\right)^4}\right]3.3^{\exp\left[\frac{-\left(0.159\omega T_p-1\right)^2}{2\sigma^2}\right]}, \tag{24}$$

in which H_s is the significant wave height defined as the mean of the one third highest waves; T_p is the spectral peak period.

$$\sigma=\begin{cases}0.07 & \text{if } \omega\le\omega_p\\ 0.09 & \text{if } \omega>\omega_p\end{cases}$$

where ω_p is the spectral peak angular frequency, $\omega_p=2\pi/T_p$.

Five wave conditions with and without forward speed are performed. Table 1 summarizes the parameters of spectra where H_s is the significant height, T_p is the wave peak period, U_0 is the forwad

speed of reference, $\min(f_e)$ and $\max(f_e)$ are the upper and lower bounds of wave frequencies. The difference between two adjacent frequencies $\mathrm{d}f_e$ .is equal to the fundamental frequency f_f :

$$\mathrm{d}f_e = f_{ei} - f_{e(i-1)} = n_i f_f - n_{i-1} f_f = (n_i - n_{i-1}) f_f = f_f \tag{25}$$

The sampling period $T_s = 1/f_f = 1/\mathrm{d}f_e$. Since $\min(f_e)$, $\max(f_e)$ and $\mathrm{d}f_e$ are based on the encounter frequency f_e, the natural wave frequency f is inversely solved by Eq. (8) first and $S(\omega)$ is obtained from Eq. (23) or Eq. (24). In additions, since the reference frame of numerical wave tank is moving with the ship, $S(\omega)$ should be converted to the domain of encounter frequency $S(\omega_e)$ by Eq. (10).

Table 1 Parameters of wave spectra

Case No.	Spectrum	H_s (m)	T_p (s)	U_0 (m/s)	min(f_e)	max(f_e)	$\mathrm{d}f_e$ (Hz)
1	JONSWAP	3.8	9.8	0	0.02	0.25	0.005
2	ISSC	3.8	9.8	5	0.02	0.58	0.01
3	JONSWAP	3.8	9.8	5	0.02	0.58	0.01
4	ISSC	8.6	13.3	5	0.02	0.45	0.01
5	JONSWAP	8.6	13.3	5	0.02	0.45	0.01

A 2D numerical wave tank is set up in this section with the length of 500 m, ranging from –100 m < x < 400 m. The depth of the tank is 100 m. The wave height probe is located at x=0. A sponge layer is set at the end of the tank with the length of 100 m. The geometry of the wave tank is demonstrated in Fig. 4.

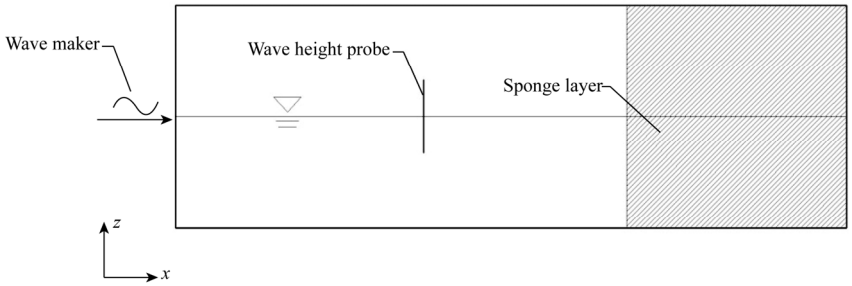

Fig. 4. Geometry of numerical wave tank.

All the meshes used in this study are generated by snappyHexMesh, a mesh generation utility provided by OpenFOAM. This utility generates mesh automatically on an original Cartesian background mesh, splitting hexahedral cells into split-hexahedra cells. It also has the capability of adding local refinement at specific regions. The mesh used in this section is shown in Fig. 5. Local refinement is applied in the surface region to improve the accuracy of surface capture. The total cell number of the 2D mesh is 21278 cells. The time step of each case is fixed at 0.01 s. Each computation in Table 1 was performed on a Xeon E5520 (2.27 GHz) cluster, using 8 processors. The computation took 20 CPU hours for each case. The simulation time was 1000 s with 100000 time steps in total.

Fig. 6 shows the time histories of the wave elevation measured by the wave height probe for all wave conditions. Case No.1 is taken as an example to demonstrate the procedure of correction. In this case, $H_s = 3.8$ m, $T_p = 9.8$ s and $U_0 = 0$. Fig. 7 illustrates the convergence process of the correcting

spectra. The initial spectrum (blue dashed line) is measured by the wave height probe (at $x = 0$) without correction procedure, showing large difference between the target spectrum. After one iteration, the spectrum is improved, but it still presents distinct discrepancy. After three iterations, the measured spectrum (red dashed line) closely matches the target. The result indicates that the convergence speed is very fast and the final spectrum shows good agreement with the target spectrum.

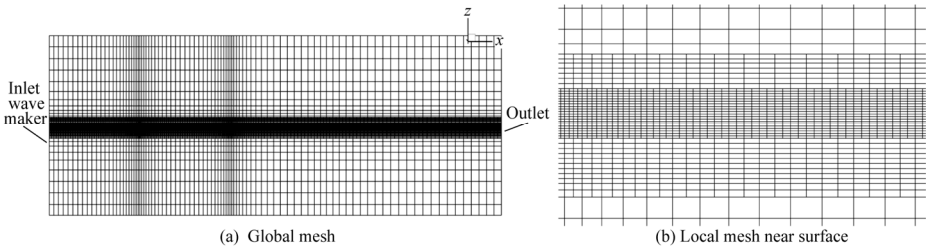

Fig. 5. Demonstration of 2D mesh used.

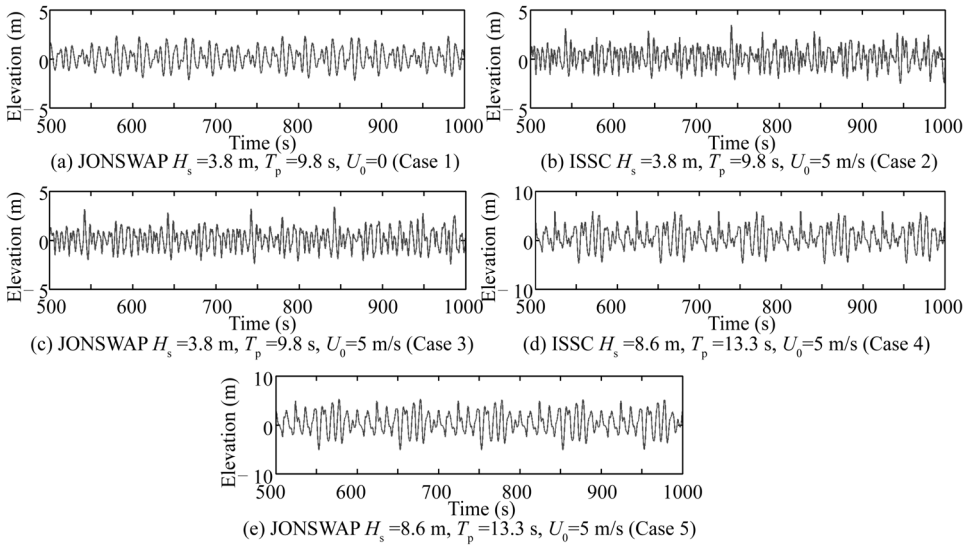

Fig. 6. Time histories of wave elevation recorded by wave height probe for all wave conditions.

Fig. 8 presents the wave elevation along the wave tank of Case 1. The results obtained by the corrected spectrum are compared with those by uncorrected spectrum. Two snapshots (t=700 and 800 s) are presented in these figures. Distinct differences between the results by two approaches can be observed. The wave elevation is dampened to zero near the location of x=350 due to the effect of the sponge layer.

Fig. 9 illustrates the comparison among uncorrected, corrected and target spectra for all other cases (Nos. 2 – 5). Similar with Case 1, the corrected spectra of all cases agree well with the targets for both ISSC and JONSWAP spectra while the initial ones, which are uncorrected, show unsatisfactory results. In additions, the presented method can obtain good agreements between corrected spectra and target for cases with not only small wave height ($H_s = 3.8$ m) but also large wave height ($H_s = 8.6$ m).

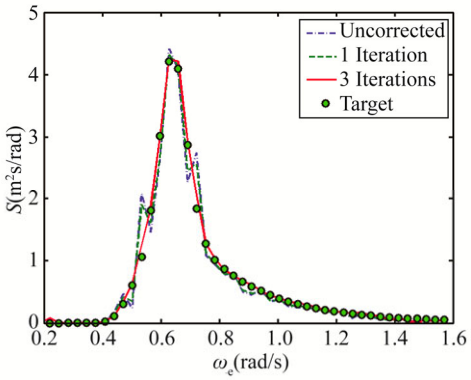

Fig. 7. Comparison of spectra with after different correcting iterations.

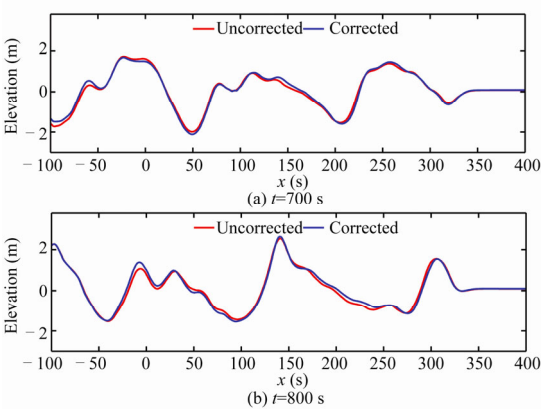

Fig. 8. Wave elevation along the 2D wave tank for Case 1.

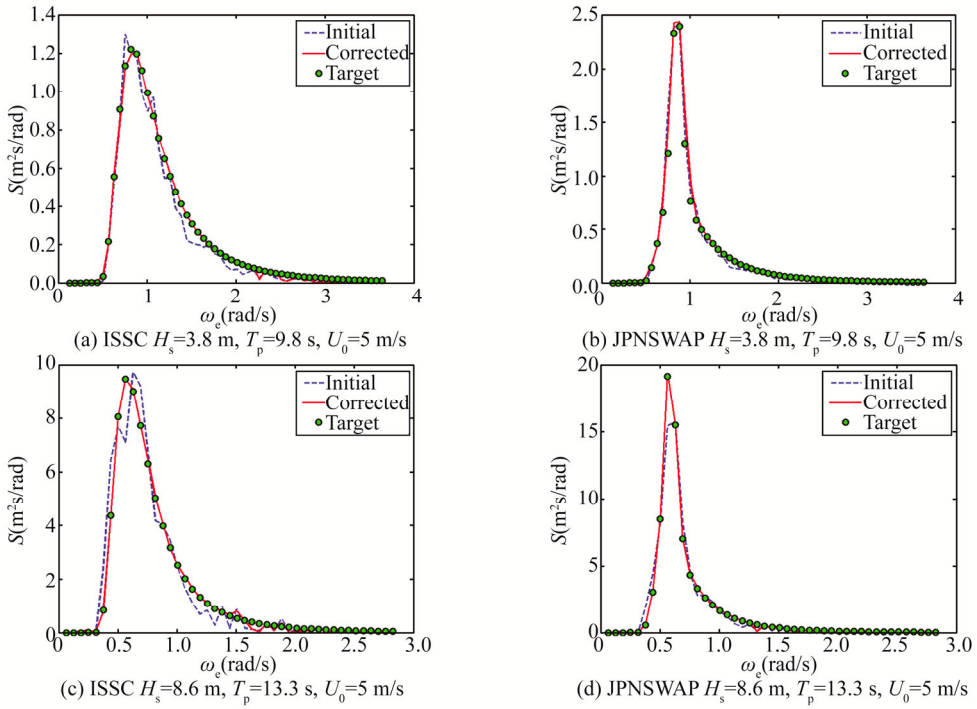

Fig. 9. The corrected measured spectra for all other wave conditions compared with targets.

Table 2 presents the comparison of the estimated significant wave height H_s', which are estimated by Eq. (26):

$$H_s' = 4.0\sqrt{m_0}\ , \tag{26}$$

where, m_0 is the area below the curve of $S(\omega_e)$:

$$m_0 = \sum_{i=1}^{n} S(\omega_{e_i})\Delta\omega_{e_i}\ . \tag{27}$$

As we can see, H_s' obtained from the corrected spectrum is much closer to the targets than that from the uncorrected ones, except for Case 1, where the corrected H_s' is over-predicted. However, although having relatively larger errors, the uncorrected H_s' are still close to the target values with the relative error smaller than 5%. The results indicate that the correction procedure can further improve the accuracy and quality of the generated irregular waves in the working region.

Table 2 Comparison of measured significant wave heights

Case	Spectrum	H_s (m)	T_p (s)	U_0 (m/s)	Estimated significant wave height, H_s' (m)		
					Uncorrected	Corrected	Target
1	JONSWAP	3.8	9.8	0	3.7909	3.8672	3.8297
2	ISSC	3.8	9.8	5	3.6783	3.7133	3.7683
3	JONSWAP	3.8	9.8	5	3.7065	3.8149	3.8293
4	ISSC	8.6	13.3	5	8.4983	8.5254	8.5584
5	JONSWAP	8.6	13.3	5	8.6081	8.7040	8.7305

3.2 Wigley Hull

In this section, the interaction between irregular waves and ship hull is investigated based on the wave generation and correction approach. The predicted motion responses are compared with the existing experiments (Journée, 1992). The experiments were performed in regular head waves, but the measured motion responses can be used for comparison. A white noise spectrum is applied to generate the irregular waves. The white noise is a spectrum in which the spectral density is uniformly distributed with constant energy. The white noise is mainly applied in signal processing but it can be used as a wave spectrum to generate irregular waves in ship and ocean engineering. Apart from the other widely used wave spectra, the white noise does not exist in natural world and it is not obtained through observation. The application of white noise is to measure the response amplitude operator (RAO) or transfer functions (TF) of floating objects. This method can replace a series of experiment tests in regular waves with a single test in irregular waves. It can largely save working time and resources. In the meanwhile, the white noise method can also achieve the same results as regular wave method does. In addition, this method can be applied to numerical wave tank in the same way as it is used in a physical wave tank. Therefore, the white noise spectrum is widely used in the marine and offshore engineering to predict the motion responses of ocean structures. Theoretically, the white noise spectrum has an infinite bandwidth. However, the motion responses of floating objects are investigated only in a specific range of frequencies. Hence, the bandwidth is truncated to a limited range of frequencies for practical use.

The expression of the white noise spectrum can be written as:

$$S(\omega_i)=\begin{cases} S_0 & \text{if } \omega_1 \le \omega_i \le \omega_2 \\ 0 & \text{if } \omega_i<\omega_1, \omega_i>\omega_2 \end{cases} \tag{28}$$

where, ω_1 and ω_2 are the lower and upper bounds of the working frequencies. S_0 is the constant spectral density in this range bounded by ω_1 and ω_2.

A modified Wigley hull is investigated in this section. Journée (1992) performed the experiments of four modified Wigley hulls in head waves. Among the modified hulls, model III is chosen in this study

because its similarity to the original hull. The principle dimensions of the hull are shown in Table 3. A 6-DoF module coupled with deforming mesh method has been developed in previous work to predict the wave induced ship motions (Shen and Wan, 2013).

Table 3 Principle dimensions of modified Wigley hull

Main particulars	Length L (m)	Breath B (m)	Draft d (m)	Displacement ∇ (m^3)	Vertical center of rotation from keel $\overline{KR}$ (m)	Vertical center of gravity from keel $\overline{KG}$ (m)	Radius of inertia k_{yy} (m)
Value	3.0000	0.3000	0.1875	0.0780	0.1875	0.1700	0.7500

The computation procedure is divided into two steps. The first step is spectrum correction, to correct the signal of input wave spectrum. In this step, a numerical wave tank without ship hull is established. A wave height probe is set up at the location of $x=1.5$ m and $y=0$ m, which is originally the ship's center of gravity. The case is carried out and the program automatically adjusts the wave generation signal. After 3 to 4 iterations, the procedure is converged and the final wave generation signal is saved.

The second step is the simulation step. A 3D numerical tank with ship hull inside is established. The ship is free to heave and pitch. This step will utilize the corrected new wave spectrum signal produced by the first step to regenerate the irregular waves. The wave heights can approach to the target values at the center of the ship. The cell spaces of the meshes and time steps in the two steps should remain unchanged to reduce the numerical error.

In this case, Fr=0.20, $S_0 = 2.5\times10^{-5}\,\mathrm{m\cdot s^2/rad}$, $0.6 \le f_e \le 1.8$ Hz and $H_s \approx 0.055$ m. The fundamental frequency $f_f = 0.1$ Hz and $T_s = 1/f_f = 10$ s. The results of the first step are shown in Fig. 10. The initial result shows moderate oscillation near the two ends of the effective range. After four iterations, the corrected result (read line) is obtained, precisely matching the target.

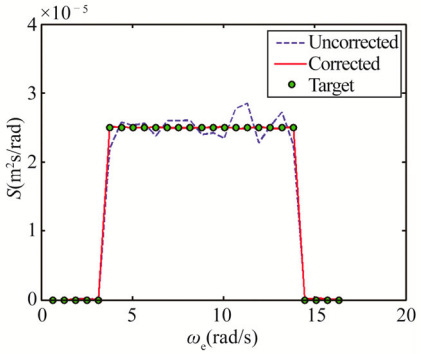

Fig. 10. Comparison among initial, corrected and target spectra.

Fig. 11 demonstrates the meshes with ship hull used in the second step. This mesh is also generated by snappyHexMesh. The cell space is close to the mesh used in the step of spectrum correction. The total cell number is around 1.5 million. The corrected wave generation signal produced by the correction step is used to generate irregular waves. The ship is free to sink and trim in the wave.

The computation was performed on a Xeon E5520 (2.27 GHz) cluster. Sixteen processors were

used for the computation. The time step was fixed at 0.001 s and the simulation time was 35 s (35000 time steps), which cost about 1600 CPU hours.

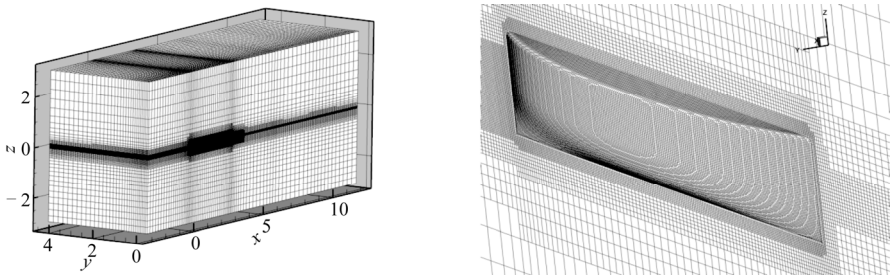

Fig. 11. Global mesh and local hull mesh.

Fig. 12 illustrates the time histories of heave and pitch motions of ship. In order to evaluate the motion responses in irregular waves, the transfer functions are used, denoted as:

$$TF_{x3_i}=\frac{X_{3_i}}{a_i},\quad TF_{x5_i}=\frac{X_{5_i}}{a_i k_i}, \tag{29}$$

where subscripts 3 and 5 stand for heave and pitch motions, respectively; the subscript i represents each wave component, $X_{m_i}\left(m=3,5\right)$ is the motion amplitudes, a_i is the wave amplitude and k_i is the wave number. X_{m_i} is obtained by Eq. (17) from the time histories of motions as shown in Fig. 12.

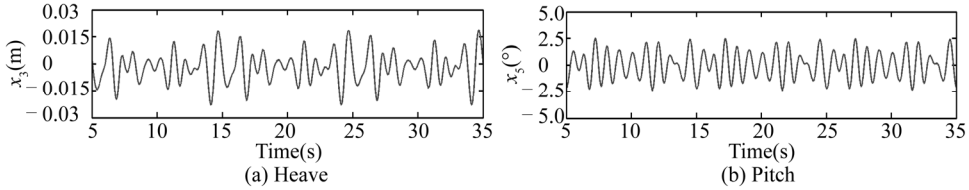

Fig. 12. Time histories of heave and pitch motions of Wigley hull in irregular head waves over $3T_s$.

At least three sampling periods T_s are provided for Fourier analysis. The results of all sampling periods are averaged. The averaged results of transfer functions are presented in Fig. 13, covering the range of all experimental data. The predicated motion responses fairly agree with the measurements, indicating good accuracy of this irregular wave procedure. Fig. 14 illustrates the free surface wave pattern at t=24.10 s.

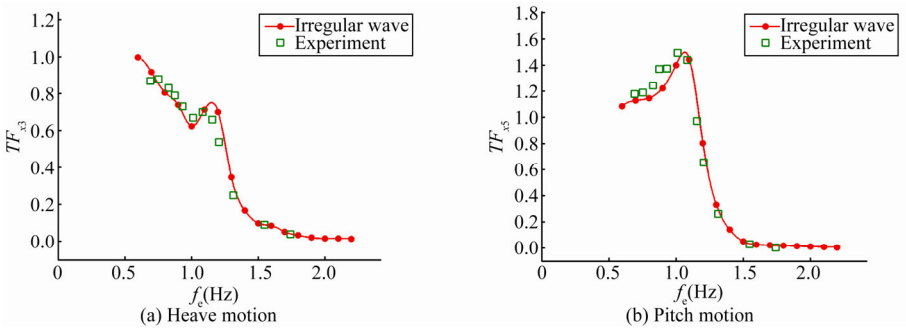

Fig. 13. Results of motion responses of heave and pitch compared with existing measurement.

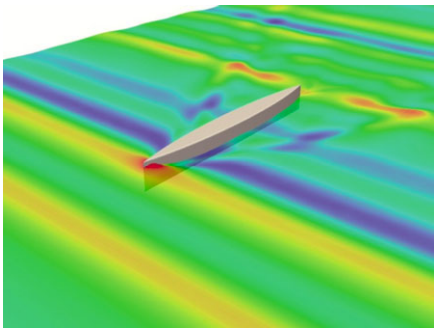

Fig. 14. Free surface field at t=24.10 s in irregular head wave.

4. Conclusions

In this work, a long-crest irregular wave generating approach in numerical wave tank using our in-house solver naoe-FOAM-SJTU was presented. Waves were generated by imposing the boundary condition of the inlet boundary condition. Different wave spectra, including JONSWAP, ISSC and white noise, were used to produce irregular waves. A correction method was implemented to correct the wave spectrum based on the measured wave elevation. Three different wave spectra with different wave heights and periods were taken for validation. The results indicated that the corrected spectrum measured by wave height probe in the numerical wave tank is greatly improved, showing better agreements with the target value than those without the correction.

A modified Wigley hull was placed in the numerical wave tank for further validation. A white noise spectrum was applied to predict transfer functions of heave and pitch motions with various encounter frequencies by a single run. In the case, Fr=0.20 and $H_s \approx 0.055$ m. The computational results show fairly good agreements with the measurements.

The computational results indicate that the irregular wave generation and correction method can produce accurate wave spectrum at the designated area and reduce the influence of numerical dissipation. It can be applied in the numerical wave tank to improve the accuracy of the simulations. In the future work, this procedure will be applied to evaluate motion responses of ships and ocean structures in irregular waves and validated with experiments.

References

Berberović, E., van Hinsberg, N., Jakirlić, S., Roisman, I. and Tropea, C., 2009. Drop impact onto a liquid layer of finite thickness: Dynamics of the cavity evolution, *Phys. Rev. E*, **79**(3): 036306.

Cao, H. J. and Wan, D. C., 2015. RANS-VOF solver for solitary wave run-up on a circular cylinder, *China Ocean Eng.*, **29**(2): 183–196.

Cao, H. J., Zha, J. J. and Wan, D. C., 2011. Numerical simulation of wave run-up around a vertical cylinder, *Proceedings of 21st International Offshore and Polar Engineering Conference*, Maui, Hawaii, USA, 726–733.

Carrica, P. M., Paik, K. J., Hosseini, H. S. and Stern, F., 2008. URANS analysis of a broaching event in irregular quartering seas, *J. Mar. Sci. Technol.*, **13**(4): 395–407.

Carrica, P. M., Wilson, R. V., Noack, R. W. and Stern, F., 2007. Ship motions using single-phase level set with

dynamic overset grids, *Comput. Fluids*, **36**(9): 1415–1433.

Chen, L. F., Zang, J., Hillis, A. J., Morgan, G. C. J. and Plummer, A. R., 2014. Numerical investigation of wave–structure interaction using OpenFOAM, *Ocean Eng.*, **88**, 91–109.

Faltinsen, O., 1993. *Sea Loads on Ships and Offshore Structures*, Cambridge University Press.

Higuera, P., Lara, J. L. and Losada, I. J., 2013. Realistic wave generation and active wave absorption for Navier–Stokes models: Application to OpenFOAM, *Coast. Eng.*, **71**, 102–118.

Issa, R. I., 1986. Solution of the implicitly discretised fluid flow equations by operator-splitting, *J. Comput. Phys.,* **62**(1): 40–65.

Jacobsen, N. G., Fuhrman, D. R. and Fredsøe, J., 2012. A wave generation toolbox for the open-source CFD library: OpenFoam, *Int. J. Numer. Methods Fluids*, **70**(9): 1073–1088.

Journée, J. M. J., 1992. *Experiments and calculations on 4 Wigley Hull Forms in Head Waves*, Report of Delft University of Technology, Ship Hydromechanics Laboratory, (No. Report 0909), The Netherlands.

Larsen, J. and Dancy, H., 1983. Open Boundaries in Short Wave Simulations—a new appraoch, *Coast. Eng.*, **7**(3): 285–297.

Menter, F. R., Kuntz, M. and Langtry, R., 2003. Ten years of industrial experience with the SST turbulence model, *Turbul. Heat Mass Transf.*, **4**(1): 625–632.

Mousaviraad, S. M., Carrica, P. M. and Stern, F., 2010. Development and validation of harmonic wave group single-run procedure for RAO with comparison to regular wave and transient wave group procedures using URANS, *Ocean Eng.*, **37**(8–9): 653–666.

Orihara, H. and Miyata, H., 2003. Evaluation of added resistance in regular incident waves by computational fluid dynamics motion simulation using an overlapping grid system, *J. Mar. Sci. Technol.*, **8**(2): 47–60.

Rhie, C. M. and Chow, W. L., 1983. Numerical study of the turbulent flow past an airfoil with trailing edge separation, *AIAA J.*, **21**(11): 1525–1532.

Rusche, H., 2002. *Computational Fluid Dynamics of Dispersed Two-Phase Flows at High Phase Fractions*, Ph.D. Thesis, Imperial College, London, UK.

Sato, Y., Miyata, H. and Sato, T., 1999. CFD simulation of 3-dimensional motion of a ship in waves: Application to an advancing ship in regular heading waves, *J. Mar. Sci. Technol.*, **4**(3): 108–116.

Shen, Z. R., Cao, H. J., Wan, D. C. and 2013. Development of CFD solver for ship and ocean engineering flows. I: *8th International OpenFOAM Workshop*, Jeju, Korea, paper No. 2F012.

Shen, Z. R. and Wan, D. C., 2013. RANS computations of added resistance and motions of a ship in head waves, *Int. J. Offshore Polar Eng.*, **23**(4): 263–271.

Shen, Z. R., Ye, H. X. and Wan, D. C., 2014. URANS simulations of ship motion responses in long-crest irregular waves, *J. Hydrodyn. Ser. B*, **26**(3): 436–446.

Yang, C., Löhner, R. and Lu, H., 2006. An unstructured-grid based volume-of-fluid method for extreme wave and freely-floating structure interactions, *J. Hydrodyn. Ser. B*, *Proceedings of the Conference of Global Chinese Scholars on Hydrodynamics*, **18**(3): 415–422.